

## Article

# Preparation of Al<sub>3</sub>Ti-Al<sub>2</sub>O<sub>3</sub>/Al Inoculant and Its Inoculation Effect on Al-Cu-Mn Alloy

Jinhua Ding<sup>1</sup>, Chao Wang<sup>1</sup>, Cheng Lu<sup>2,\*</sup>, Guangming Zhu<sup>1</sup>, Nana Guo<sup>1</sup>, Xujie Gao<sup>1</sup>, Xin Wang<sup>3,\*</sup>   
and Chunxiang Cui<sup>3</sup>

<sup>1</sup> School of Mechanical Engineering, Shandong University of Technology, Zibo 255000, China

<sup>2</sup> School of Physics and Optoelectronic Engineering, Shandong University of Technology, Zibo 255000, China

<sup>3</sup> Hebei Key Laboratory of New Functional Materials, School of Material Science and Engineering, Hebei University of Technology, Tianjin 300401, China

\* Correspondence: luchengcg@163.com (C.L.); ahaxin@hebut.edu.cn (X.W.);

Tel.: +86-0533-2786-815 (C.L.); +86-022-6020-4125 (X.W.)

**Abstract:** The grain size plays a pivotal role in determining the properties of the alloy. The grain size can be significantly decreased by adding inoculants. Aiming to address the shortcomings of existing inoculants, the Al<sub>3</sub>Ti-Al<sub>2</sub>O<sub>3</sub>/Al inoculant was successfully prepared using Al-Ti master alloy and Al<sub>2</sub>O<sub>3</sub> whiskers as raw materials. With the aid of ultrasonic energy, the Al<sub>2</sub>O<sub>3</sub> whiskers were uniformly dispersed within the inoculants. Under the combined action of ultrasonic and titanium, the Al<sub>2</sub>O<sub>3</sub> whiskers were broken into small particles at high temperature. To enhance the morphology of Al<sub>3</sub>Ti and achieve even particle dispersion throughout the matrix, vacuum rapid quenching treatment was applied to the inoculant. The SEM test results indicated a significant reduction in particle size after vacuum rapid quenching. The Al<sub>3</sub>Ti-Al<sub>2</sub>O<sub>3</sub>/Al inoculants exhibited excellent grain refinement effects on the weldable Al-Cu-Mn alloy. Crystallographic calculations and HRTEM analysis revealed that Al<sub>2</sub>O<sub>3</sub> and Al have orientation relationships, indicating their potential as effective heterogeneous nucleation sites. The mechanical properties of the Al-Cu-Mn alloy were obviously improved after the Al<sub>3</sub>Ti-Al<sub>2</sub>O<sub>3</sub>/Al inoculant was added.

**Keywords:** inoculant; Al<sub>2</sub>O<sub>3</sub> whiskers; grain refinement; microstructure; property



**Citation:** Ding, J.; Wang, C.; Lu, C.; Zhu, G.; Guo, N.; Gao, X.; Wang, X.; Cui, C. Preparation of Al<sub>3</sub>Ti-Al<sub>2</sub>O<sub>3</sub>/Al Inoculant and Its Inoculation Effect on Al-Cu-Mn Alloy. *Materials* **2023**, *16*, 5264. <https://doi.org/10.3390/ma16155264>

Academic Editor: Andrey Belyakov

Received: 29 June 2023

Revised: 17 July 2023

Accepted: 20 July 2023

Published: 27 July 2023



**Copyright:** © 2023 by the authors. Licensee MDPI, Basel, Switzerland. This article is an open access article distributed under the terms and conditions of the Creative Commons Attribution (CC BY) license (<https://creativecommons.org/licenses/by/4.0/>).

## 1. Introduction

The refinement of grain is widely acknowledged as a straightforward and efficient approach to enhance the microstructure and properties of aluminum alloys [1–5]. Grain refinement can be achieved through adding inoculants, increasing melt cooling rate, stirring, ultrasonic treatment, plastic deformation and heat treatment [6–10]. Among these refining methods, adding inoculants to aluminum alloy melt is the most simple and effective method. The inoculants of aluminum alloy mainly include some alloying elements and ceramic particles [11–14]. Alloying elements usually play a role in heterogeneous nucleation of Al matrix by forming intermetallic compounds with Al. The main requirements for ceramic inoculants are high melting points, excellent physical and chemical stability, and low lattice misfit with the substrates [15–20].

For most aluminum alloys, the Al-5Ti-B refiner can play a role in grain refinement. However, in the Al-5Ti-B ingot, TiB<sub>2</sub> particles tend to aggregate and form clusters, and the Al<sub>3</sub>Ti phase is usually needle-like, which are detrimental to the refinement effect. Moreover, the presence of elements such as Zr, Si, Cr, and V in aluminum alloy can lead to a “poisoning” effect on Al-5Ti-B [21–24]. For instance, even 0.2 wt.% of Zr can rapidly diminish the refining capability of Al-5Ti-B. The reason is the formation of (Ti<sub>1-x</sub>Zr<sub>x</sub>)Al<sub>3</sub> and (Ti<sub>1-x</sub>Zr<sub>x</sub>)B<sub>2</sub>, which leads to the weakening of heterogeneous nucleation ability of TiB<sub>2</sub> and Al<sub>3</sub>Ti particles. Additionally, the formation of (Ti<sub>1-x</sub>Zr<sub>x</sub>)Al<sub>3</sub> weakens the constraining

effect of free Ti on grain growth, while Zr disrupts the two-dimensional monatomic layer of  $\text{Al}_3\text{Ti}$  on the surface of  $\text{TiB}_2$ , resulting in a loss of grain refinement effectiveness [25–27].

Then, Al-Ti-B-RE [28,29] was developed to further improve the refining effect of Al-Ti-B refiner. The addition of rare earth can not only change the morphology of  $\text{Al}_3\text{Ti}$  particles but also improve the dispersibility of  $\text{TiB}_2$  and  $\text{Al}_3\text{Ti}$  particles and increase the degree of supercooling of aluminum melt. Compared with the traditional Al-Ti-B refiner, Al-Ti-B-RE refiner has a better refining effect, but its optimization effect is limited, the process is complicated and the cost is high.

Al-Ti-C intermediate alloy is also an aluminum alloy refiner widely used in industrial production. In crystallography, there exists a specific orientation relationship between TiC particles and the  $\alpha$ -Al matrix, and so, it has heterogeneous nucleation potential for  $\alpha$ -Al. Li et al. [30] found that the dispersion of TiC in aluminum matrix is obviously better than that of  $\text{TiB}_2$  particles, and the particle size of TiC is much smaller than that of  $\text{TiB}_2$ . Therefore, for two kinds of particles with the same mass fraction, the number of TiC particles is more than that of  $\text{TiB}_2$ , so that more nucleation sites can be provided for  $\alpha$ -Al, thus achieving a better refining effect. However, the major disadvantage of Al-Ti-C is that TiC and Al will react to form  $\text{Al}_4\text{C}_3$  brittle phase at a certain temperature:  $13\text{Al}(\text{l}) + 3\text{TiC}(\text{s}) = 3\text{TiAl}_3(\text{s}) + \text{Al}_4\text{C}_3(\text{s})$  [31], resulting in poor stability of TiC and fading behaviors of the refinement effect. In addition, the preparation of Al-Ti-C refiner is usually based on graphite powder, carbon tetrachloride and other carbon sources, which are added to the Al-Ti intermediate alloy melt at high temperature and then reacted with each other. However, due to the poor wettability of carbon in aluminum, the low utilization rate of C and the high reaction temperature, the required preparation equipment is complicated and the cost is high. Therefore, Al-Ti-C refiner cannot be used on a large scale in industrial production [32].

In order to improve the refining effect of Al-Ti-C refiner, Zhao, Ding and Xu et al. [33,34] prepared Al-Ti-C-RE refiner. After the addition of rare earth elements, the wettability of C and Al melt is improved, which promotes the formation of TiC particles. In addition, rare earth can improve the morphology of  $\text{Al}_3\text{Ti}$  particles, reduce the size of  $\text{Al}_3\text{Ti}$  particles, improve the dispersion of TiC and  $\text{Al}_3\text{Ti}$  particles and improve the refining effect and property of anti-degeneration of refiners. However, the development of Al-Ti-C-RE refiner is the same as that of Al-Ti-B-RE refiner, with limited optimization effect, cumbersome process and high cost [35–37]. Therefore, it is necessary to develop new inoculants to overcome the shortcomings of existing inoculants.

$\alpha$ - $\text{Al}_2\text{O}_3$  belongs to the trigonal system and is composed of hexagonal tightly packed crystals. The lattice constant of  $\alpha$ - $\text{Al}_2\text{O}_3$  is  $a = b = 0.4759$  nm,  $c = 1.3$  nm. According to the edge-to-edge model proposed by Zhang et al. [17], the orientation relationships between  $\alpha$ -Al and  $\alpha$ - $\text{Al}_2\text{O}_3$  are as follows:  $(200)_{\text{Al}} \parallel (006)_{\text{Al}_2\text{O}_3}$ ,  $[011]_{\text{Al}} \parallel [\bar{1}20]_{\text{Al}_2\text{O}_3}$ ;  $(200)_{\text{Al}} \parallel (006)_{\text{Al}_2\text{O}_3}$ ,  $[011]_{\text{Al}} \parallel [\bar{1}10]_{\text{Al}_2\text{O}_3}$ ;  $(111)_{\text{Al}} \parallel (011)_{\text{Al}_2\text{O}_3}$ ,  $[01\bar{1}]_{\text{Al}} \parallel [11\bar{1}]_{\text{Al}_2\text{O}_3}$ . In addition,  $\alpha$ - $\text{Al}_2\text{O}_3$  has the advantages of high strength, high melting point, high elastic modulus and good stability [38–42]; as a result, it can serve as heterogeneous substrates for  $\alpha$ -Al and effectively refine aluminum alloys. In this paper, we desired to replace  $\text{TiB}_2$  with  $\text{Al}_2\text{O}_3$  to overcome the shortcomings of the existing inoculants.

The wettability between  $\alpha$ - $\text{Al}_2\text{O}_3$  particles and liquid aluminum is poor, and so, it is easy to aggregate into clusters on the surface of liquid aluminum. In this paper, the  $\text{Al}_2\text{O}_3$  whiskers instead of  $\text{Al}_2\text{O}_3$  particles were added to the liquid Al-Ti master alloy at high temperature, and ultrasonic treatment was used to improve the dispersion and wettability.

## 2. Materials and Methods

The primary equipment utilized in the preparation of Al-Cu-Mn alloy was predominantly the MZG series high-frequency induction melting furnace. First, commercial pure aluminum (99 wt.%), commercial pure copper (99 wt.%), commercial pure zinc (99 wt.%), Al-Mn, Al-Ti, Al-Zr and Al-V were proportionally weighed using an electronic scale. The weighed pure aluminum and pure copper were placed in the graphite crucible and heated in the MZG series high-frequency induction melting furnace. After these two metals were

melted, the weighed commercial pure zinc (99 wt.%), Al-Mn, Al-Ti, Al-Zr and Al-V were quickly put in and fully stirred with graphite rods. After all the raw materials were melted and fully stirred, the dross on the surface of the molten liquid was removed with a scraping spoon and was then poured into the preheated steel mold to produce alloy sample rods with  $\Phi 20 \text{ mm} \times 100 \text{ mm}$ .

The raw materials for preparation of  $\text{Al}_3\text{Ti-Al}_2\text{O}_3/\text{Al}$  inoculant were Al-Ti master alloy and alumina whiskers. The alumina whiskers were provided by the Shenzhen Research Institute of Tsinghua University (Shenzhen, China). The Al-Ti master alloy was melted in a high frequency induction furnace, and then the alumina whiskers were added to the melt in a certain proportion. To make the whisker evenly dispersed in the melt, ultrasonic vibration treatment was applied to the melt, and the metal liquid was then cast into the steel mold. To achieve a uniform dispersion of the inoculant in the Al-Cu-Mn matrix alloy, the inoculant ingots were remelted and transformed into ribbons through vacuum rapid quenching, that is, by pouring liquid metal on a spinning cold copper wheel.

The Al-Cu-Mn alloy was melted at  $800^\circ\text{C}$  in the crucible resistance furnace. After the Al-Cu-Mn alloy was melted, the inoculant ribbons were added to the melt and thoroughly stirred with a graphite rod and were then cast into the steel mold of  $\Phi 20 \text{ mm} \times 100 \text{ mm}$ . The Al-Cu-Mn alloys underwent T6 heat treatment, which involved solution treatment at  $520^\circ\text{C}$  for 24 h followed by water quenching and artificial aging treatment at  $165^\circ\text{C}$  for 14 h.

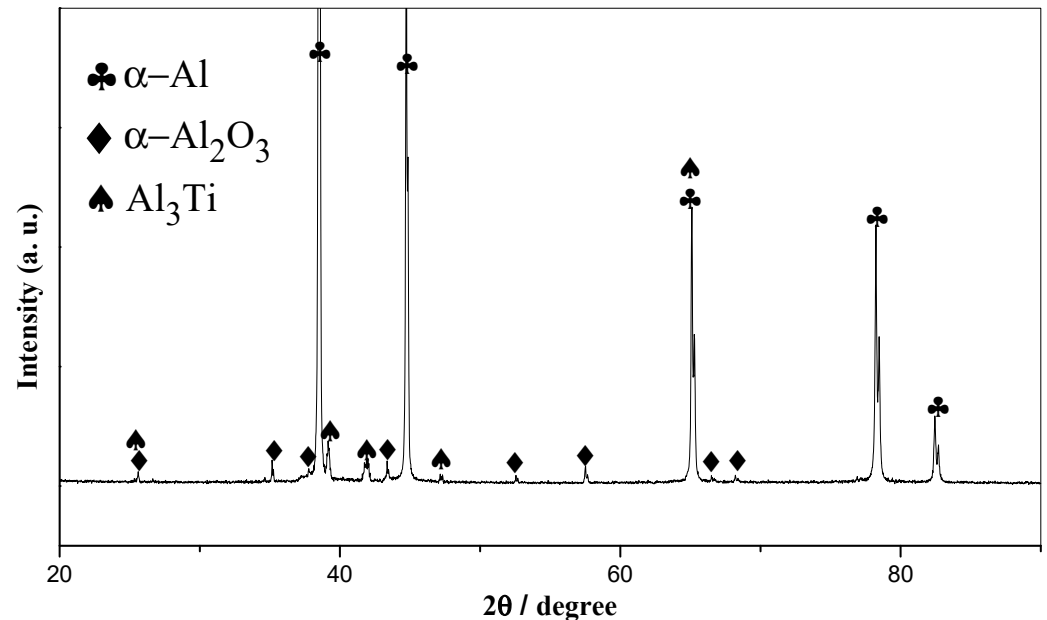
The phase composition of the inoculants was determined via X-ray diffraction (XRD). The metallographic microscope was utilized to observe the changes in grain morphology and size. The microstructures and element composition of the alloy and inoculant were analyzed by the scanning electron microscopy (SEM) equipped with energy dispersive X-ray spectroscopy (EDS). To enable observation of the sample under both optical and scanning electron microscopes, it underwent a series of preparation steps including sandpaper polishing with varying roughness, mechanical polishing using a specialized machine and, finally, corrosion treatment utilizing Keller reagent. The heterogeneous nucleation particles in alloy were characterized using JEM-2100 F (JEOL, Tokyo, Japan) transmission electron microscope (TEM). The specimens for TEM observation were prepared by ion milling. The mechanical properties of the alloy was measured using a universal testing machine.

### 3. Results and Discussion

The XRD pattern of  $\text{Al}_3\text{Ti-Al}_2\text{O}_3/\text{Al}$  inoculant is presented in Figure 1, revealing that the phase composition of the inoculant primarily comprised  $\alpha\text{-Al}$ ,  $\alpha\text{-Al}_2\text{O}_3$  and  $\text{Al}_3\text{Ti}$ .

The SEM images of  $\text{Al}_3\text{Ti-Al}_2\text{O}_3/\text{Al}$  inoculants and the EDS patterns of the second phases are presented in Figure 2. The matrix contained distributed rod-like and granular second phases, as illustrated in Figure 2a. In Figure 2b, it can be seen that the granular second phases were nanometer and submicron in size. The rod-like second phases were alumina whiskers, and it can be found that there were craters on the surface of the alumina whiskers and the whisker length was obviously reduced. At high temperature ( $1600\sim 1700^\circ\text{C}$ ),  $\text{Al}_2\text{O}_3$  will decompose and release O atoms, the O atoms can easily combine with the Ti atoms in the melt to form  $\text{TiO}_2$  or  $\text{Al}_2\text{TiO}_5$  [43–45]. However, no diffraction peaks corresponding to other phases were observed in the XRD pattern shown in Figure 1, probably because too few reaction products were generated to be detected. Because  $\text{Al}_2\text{O}_3$  can react with titanium at high temperatures, titanium in the Al-Ti master alloy will corrode the whisker and break it. The EDS pattern of point B indicates that the particles in Figure 2b were the chips dropped from the alumina whiskers after being fragmented. The gray phases in Figure 2a,b are  $\text{Al}_3\text{Ti}$ , and it can be seen that before the vacuum rapid quenching treatment, its morphology was short rod. The refining effect of large particles was less than ideal when compared to that of fine particles. Therefore, to achieve optimal refining results, the inoculant ingot was rapidly quenched under vacuum conditions. The SEM image of the  $\text{Al}_3\text{Ti-Al}_2\text{O}_3/\text{Al}$  ribbon in Figure 2f reveals a disappearance of large rod-like  $\text{Al}_3\text{Ti}$  particles and an emergence of numerous gray nanoparticles. In the process of remelting, the  $\text{Al}_3\text{Ti}$

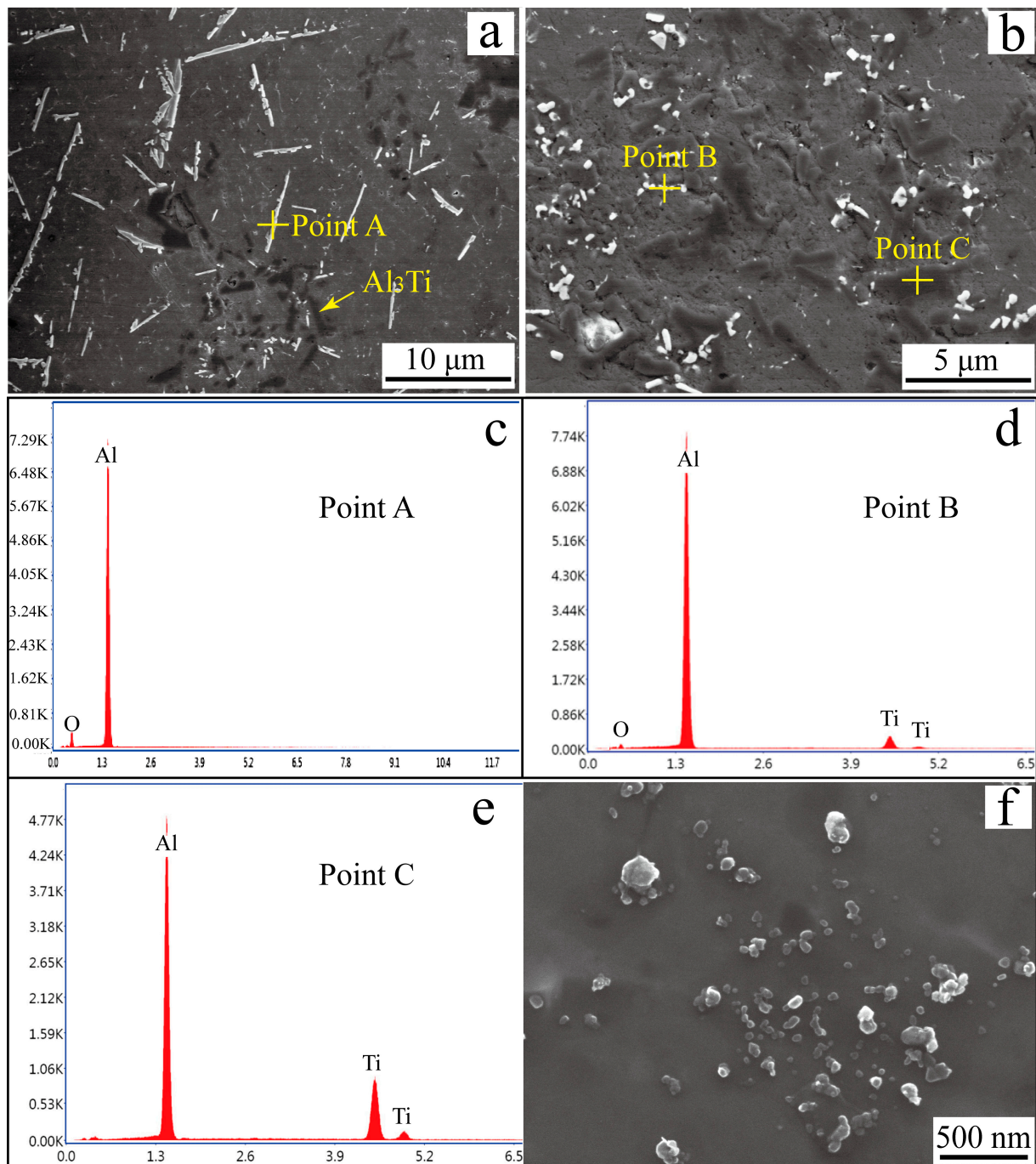
particles were dissolved in liquid aluminum. In the subsequent solidification stage, due to the rapid cooling rate, these particles did not have sufficient time to grow and, thus, resulted in the formation of numerous nanoparticles.



**Figure 1.** XRD pattern of  $\text{Al}_3\text{Ti-Al}_2\text{O}_3/\text{Al}$  inoculant.

To evaluate the refining effect of  $\text{Al}_3\text{Ti-Al}_2\text{O}_3/\text{Al}$  inoculant on Al-Cu-Mn alloy, 1 wt.% of the inoculant was introduced into the alloy. The metallographic images of the Al-Cu-Mn alloy, both pre- and post-inoculation, are depicted in Figure 3. The addition of the inoculant resulted in a significant reduction in grain size for the Al-Cu-Mn alloy. The main reasons for the decrease in the grain size after adding  $\text{Al}_3\text{Ti-Al}_2\text{O}_3/\text{Al}$  inoculant were as follows: first,  $\text{Al}_3\text{Ti}$  can serve as a heterogeneous nucleation site for  $\alpha\text{-Al}$ ; second, Ti can limit the growth of aluminum grains; third, the calculation results show that  $\text{Al}_2\text{O}_3$  and Al also had crystal orientation relationships and, therefore, it can serve as a site for heterogeneous nucleation of  $\alpha\text{-Al}$  during the solidification process of the alloy.

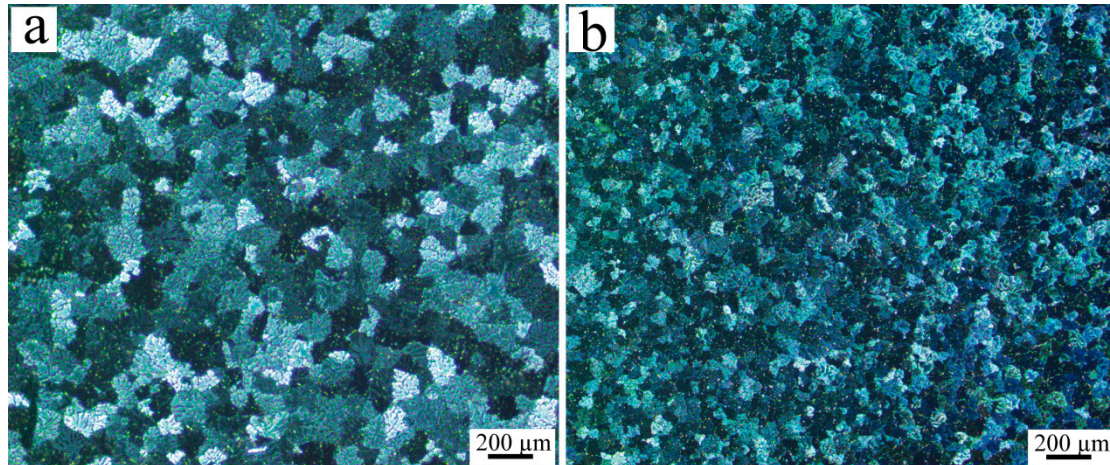
The (111), (200) and (220) planes of Al corresponded to the first, second and third close-packed planes, respectively, with interplanar spacings of 0.234 nm, 0.202 nm and 0.143 nm. The close-packed crystallographic planes of  $\text{Al}_2\text{O}_3$  were (012), (104), (110) and (006) with corresponding interplanar spacings of 0.348 nm, 0.255 nm, 0.238 nm and 0.217 nm, respectively. By calculating, Al and  $\text{Al}_2\text{O}_3$  can form the following orientation relationships:  $(111)_{\text{Al}} // (110)_{\text{Al}_2\text{O}_3}$ ,  $[011]_{\text{Al}} // [111]_{\text{Al}_2\text{O}_3}$ ;  $(200)_{\text{Al}} // (006)_{\text{Al}_2\text{O}_3}$ ,  $[011]_{\text{Al}} // [\bar{1}20]_{\text{Al}_2\text{O}_3}$ ;  $(200)_{\text{Al}} // (006)_{\text{Al}_2\text{O}_3}$ ,  $[011]_{\text{Al}} // [1\bar{1}0]_{\text{Al}_2\text{O}_3}$ . The Materials Studio (MS 7.0) software was utilized to generate a schematic diagram illustrating the lattice matching between  $\text{Al}_2\text{O}_3$  and Al, as depicted in Figure 4. In Figure 4(a<sub>1</sub>,a<sub>2</sub>), it can be seen the crystal plane spacing of  $(111)_{\text{Al}}$  was close to that of  $(110)_{\text{Al}_2\text{O}_3}$ , the atomic spacing of  $[011]_{\text{Al}}$  was close to that of  $[111]_{\text{Al}_2\text{O}_3}$ ; therefore, they can form a good interface combination in theory. In Figure 4(b<sub>1</sub>–b<sub>3</sub>), it can be seen that when the  $(200)_{\text{Al}}$  was combined with the  $(006)_{\text{Al}_2\text{O}_3}$ , the plane spacing between them and the atomic spacing of the corresponding crystal orientation were very close, and so,  $(200)_{\text{Al}}$  and  $(006)_{\text{Al}_2\text{O}_3}$  also can form a good interface combination in theory.



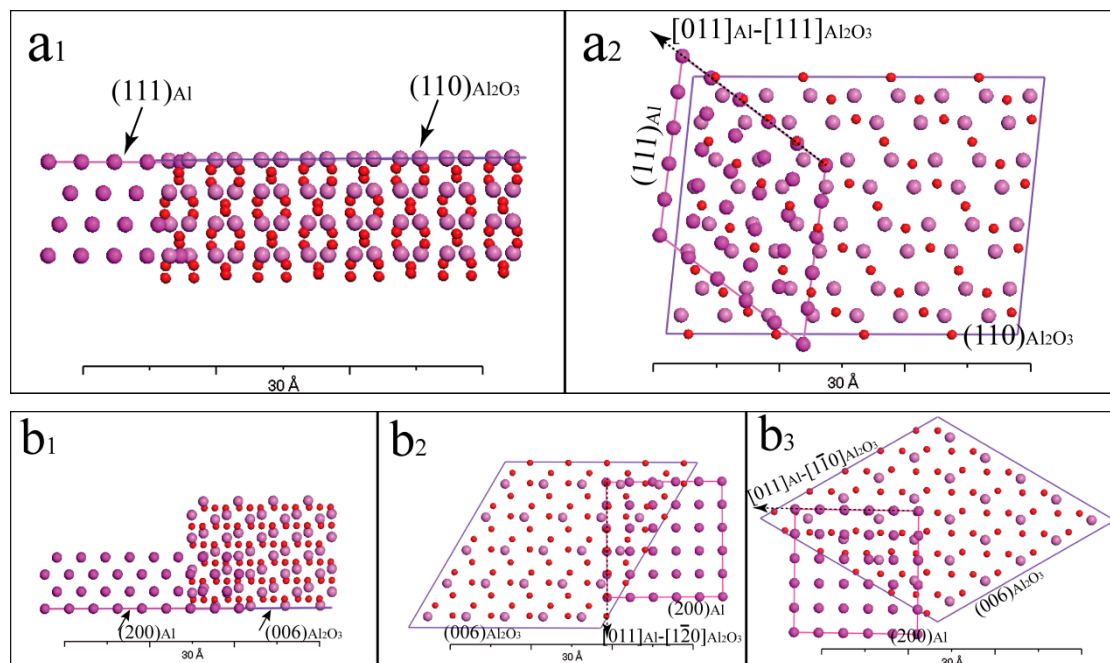
**Figure 2.** (a,b) SEM images of  $\text{Al}_3\text{Ti-Al}_2\text{O}_3/\text{Al}$  inoculants, (c) EDS pattern of Point A, (d) EDS pattern of Point B, (e) EDS pattern of Point C, (f) SEM image of  $\text{Al}_3\text{Ti-Al}_2\text{O}_3/\text{Al}$  inoculant after vacuum rapid quenching.

The HRTEM image of the Al-Cu-Mn alloy inoculated with the  $\text{Al}_3\text{Ti-Al}_2\text{O}_3/\text{Al}$  inoculant is presented in Figure 5c, revealing a slight variation in atomic arrangement within the circular box region compared to its surrounding area. The measurement results show that the interplanar spacing  $d_1$  was 0.2134 nm and  $d_2$  was 0.2505 nm, and the angle between the two crystallographic planes was  $38.54^\circ$ . Figure 5a is the simulation of  $\text{Al}_2\text{O}_3$  lattice built by MS 7.0 software. Figure 5b is the simulation of (104) and (006) planes cut from  $\text{Al}_2\text{O}_3$  lattice, the plane spacing of (104) and (006) was 0.255 nm and 0.217 nm, respectively, and the angle between them was  $38.2^\circ$ . It indicates that the phase of the round frame region corresponded to the  $\text{Al}_2\text{O}_3$ , and so, the round frame area can be identified as  $\text{Al}_2\text{O}_3$ . Figure 5d–f depict

the fast Fourier transform (FFT) patterns of zones A, B and C. As evidenced by the HRTEM image and FFT pattern, the  $(006)_{\text{Al}_2\text{O}_3}$  plane was parallel to  $(200)_{\text{Al}}$  with closely matched plane spacing. The analysis results indicate that a perfect interface can be formed between  $\text{Al}_2\text{O}_3$  and Al, thus enabling  $\text{Al}_2\text{O}_3$  to serve as the heterogeneous nucleation site for Al. These test findings are consistent with the aforementioned theoretical analysis.



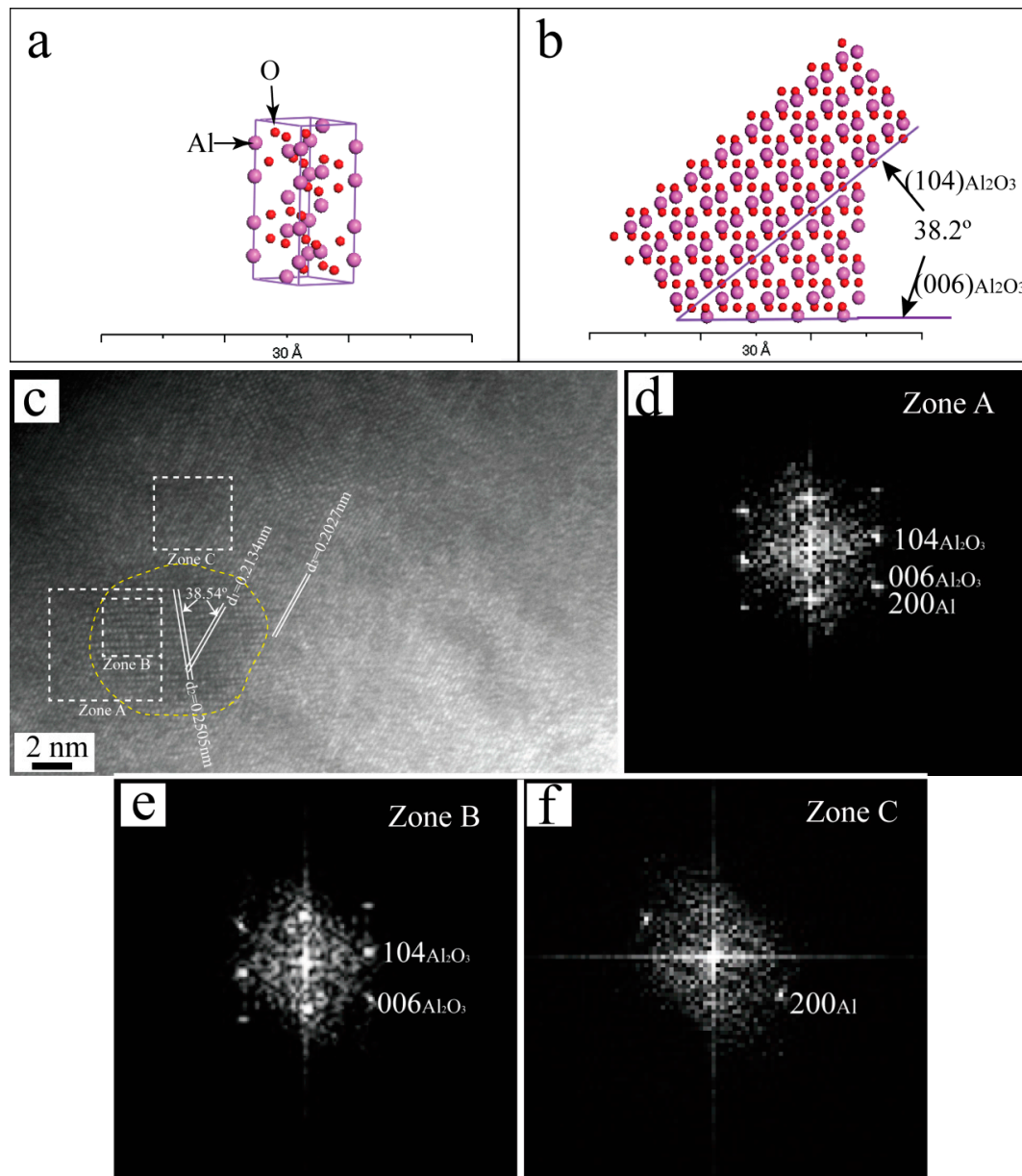
**Figure 3.** Metallographic image of (a) Al-Cu-Mn alloy, (b) Al-Cu-Mn alloy inoculated by  $\text{Al}_3\text{Ti-Al}_2\text{O}_3/\text{Al}$ .



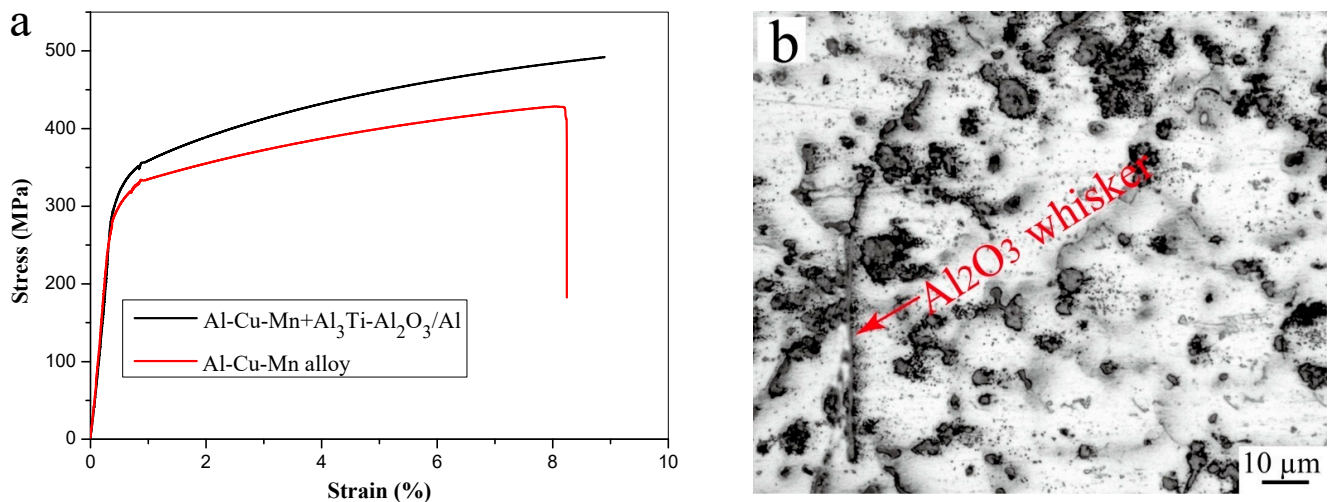
**Figure 4.** Schematic diagram of the lattice matching between Al and  $\text{Al}_2\text{O}_3$ . (a<sub>1</sub>)  $(111)_{\text{Al}}// (110)_{\text{Al}_2\text{O}_3}$ ; (a<sub>2</sub>)  $[011]_{\text{Al}}// [111]_{\text{Al}_2\text{O}_3}$ ; (b<sub>1</sub>)  $(200)_{\text{Al}}// (006)_{\text{Al}_2\text{O}_3}$ ; (b<sub>2</sub>)  $[011]_{\text{Al}}// [120]_{\text{Al}_2\text{O}_3}$ ; (b<sub>3</sub>)  $[011]_{\text{Al}}// [110]_{\text{Al}_2\text{O}_3}$ .

Figure 6a illustrates the stress–strain behavior of Al-Cu-Mn alloy and Al-Cu-Mn alloy treated with the  $\text{Al}_3\text{Ti-Al}_2\text{O}_3/\text{Al}$  inoculant. The enhancement of the ultimate tensile strength and a slight increase in elongation were evidently observed in the alloy. The Al-Cu-Mn alloy exhibited an initial tensile strength of 428 MPa and an elongation of 8.2%. Upon inoculation with the  $\text{Al}_3\text{Ti-Al}_2\text{O}_3/\text{Al}$  inoculant, the ultimate tensile strength was enhanced to 492 MPa, while the elongation increased to 8.8%. According to Figure 3, the addition of  $\text{Al}_3\text{Ti-Al}_2\text{O}_3/\text{Al}$  inoculants resulted in a significant reduction in the average grain size of Al-Cu-Mn alloy, leading to an increase in grain boundaries. During plastic deformation

of the alloy, the presence of grain boundaries impeded dislocation movement, thereby increasing the tensile strength of the alloy. In addition, the  $\text{Al}_3\text{Ti}$  and  $\text{Al}_2\text{O}_3$  particles can also act as the obstacles to the dislocation motion, thus leading to higher tensile strength. The alloy could maintain good plasticity while the tensile strength was increased, on the one hand because the grain refinement made the applied stress more evenly dispersed in each grain and, thus, not making it easy to form stress concentration. On the other hand, unreacted  $\text{Al}_2\text{O}_3$  whiskers can serve as a bridging agent in the matrix (as illustrated in Figure 6b), thereby contributing positively to the plasticity of the alloy.



**Figure 5.** (a,b)  $\text{Al}_2\text{O}_3$  lattice and crystal plane simulation diagrams, (c) HRTEM image of  $\text{Al}_2\text{O}_3$  particle, (d–f) fast Fourier transform (FFT) patterns of zone A, zone B and zone C.



**Figure 6.** (a) Stress–strain curves of Al-Cu-Mn alloy and Al-Cu-Mn alloy + Al<sub>3</sub>Ti-Al<sub>2</sub>O<sub>3</sub>/Al inoculant, (b) metallographic image of Al-Cu-Mn alloy inoculated by Al<sub>3</sub>Ti-Al<sub>2</sub>O<sub>3</sub>/Al.

#### 4. Conclusions

In this study, the Al<sub>3</sub>Ti-Al<sub>2</sub>O<sub>3</sub>/Al inoculant was prepared with Al-Ti master alloy and Al<sub>2</sub>O<sub>3</sub> whiskers as raw materials. The Al<sub>3</sub>Ti-Al<sub>2</sub>O<sub>3</sub>/Al inoculants were used to inoculate the Al-Cu-Mn alloy and showed good grain refining effect. The key findings can be succinctly summarized as follows:

- (1) Under the combined action of high temperature, ultrasonic and Ti element, parts of the Al<sub>2</sub>O<sub>3</sub> whiskers were fragmented into granular form. After the vacuum-quenching treatment, the large sizes Al<sub>3</sub>Ti were replaced by small size particles.
- (2) There exist orientation relationships between  $\alpha$ -Al<sub>2</sub>O<sub>3</sub> particles and the aluminum matrix, whereby the former can serve as heterogeneous nucleation substrates for the latter. The Al<sub>3</sub>Ti-Al<sub>2</sub>O<sub>3</sub>/Al inoculants exhibited a significant grain refining effect on the Al-Cu-Mn alloy.
- (3) The tensile strength of the Al-Cu-Mn alloy was improved from 428 MPa to 492 MPa and the elongation was enhanced from 8.2% to 8.8% after being inoculated by the Al<sub>3</sub>Ti-Al<sub>2</sub>O<sub>3</sub>/Al inoculants.

**Author Contributions:** Conceptualization, J.D.; methodology, C.L.; software, J.D.; validation, J.D., N.G. and X.G.; formal analysis, N.G.; investigation, C.W.; resources, G.Z.; data curation, J.D.; writing—original draft preparation, C.W. and X.W.; writing—review and editing, J.D. and G.Z.; visualization, X.W.; supervision, C.C.; project administration, G.Z. and C.C.; funding acquisition, C.L. All authors have read and agreed to the published version of the manuscript.

**Funding:** This research was funded by the Natural Science Foundation of Shandong Province, grant number ZR2021QE190 and No. ZR2021QE178.

**Institutional Review Board Statement:** Not applicable.

**Informed Consent Statement:** Not applicable.

**Data Availability Statement:** Any further detailed data may be obtained from the authors upon a reasonable request.

**Conflicts of Interest:** The authors declare no conflict of interest.

#### References

1. Zhang, L.L.; Jiang, H.X.; He, J.; Zhao, J.Z. Improved grain refinement in aluminium alloys by re-precipitated TiB<sub>2</sub> particles. *Mater. Lett.* **2022**, *312*, 131657. [[CrossRef](#)]
2. Li, J.H.; Hage, F.S.; Ramasse, Q.M.; Schumacher, P. The nucleation sequence of  $\alpha$ -Al on TiB<sub>2</sub> particles in Al-Cu alloys. *Acta Mater.* **2021**, *206*, 116652. [[CrossRef](#)]

3. Huang, B.; Liu, Y.Z.; Zhou, Z.G.; Cheng, W.; Liu, X.H. Selective laser melting of 7075 aluminum alloy inoculated by Al–Ti–B: Grain refinement and superior mechanical properties. *Vacuum* **2022**, *200*, 111030. [[CrossRef](#)]
4. Liu, X.H.; Liu, Y.Z.; Zhou, Z.G.; Wang, K.D.; Zhan, Q.K.; Xiao, X.J. Grain refinement and crack inhibition of selective laser melted AA2024 aluminum alloy via inoculation with TiC–TiH<sub>2</sub>. *Mater. Sci. Eng. A* **2021**, *813*, 141171. [[CrossRef](#)]
5. Guo, Y.W.; Wei, W.; Shi, W.; Zhang, B.; Zhou, X.R.; Wen, S.P.; Wu, X.L.; Gao, K.Y.; Rong, L.; Huang, H.; et al. Effect of Er and Zr additions and aging treatment on grain refinement of aluminum alloy fabricated by laser powder bed fusion. *J. Alloys Compd.* **2022**, *912*, 165237. [[CrossRef](#)]
6. Sigworth, G.K.; Kuhn, T.A. Grain Refinement of Aluminum Casting Alloys. *Int. J. Metalcast.* **2007**, *1*, 31–40. [[CrossRef](#)]
7. Samuel, F.H.; Champier, G. Grain Refinement in Aluminum Alloys by Rapid Solidification. *Mater. Sci. Forum* **1992**, *94–96*, 747–752. [[CrossRef](#)]
8. Ghadimi, H.; Hossein, S.; Nedjhd, B. Eghbali, Enhanced grain refinement of cast aluminum alloy by thermal and mechanical treatment of Al-5Ti-B master alloy. *Trans. Nonferrous Met. Soc.* **2013**, *23*, 1563–1569. [[CrossRef](#)]
9. Qiu, K.; Wang, R.C.; Peng, C.Q.; Wang, N.G.; Cai, Z.Y.; Zhang, C. Effects of Mn and Sn on microstructure of Al-7Si-Mg alloy modified by Sr and Al-5Ti-B. *Trans. Nonferrous Met. Soc.* **2015**, *25*, 3546–3552. [[CrossRef](#)]
10. Kai, X.Z.; Tian, K.L.; Wang, C.M.; Jiao, L.; Chen, G.; Zhao, Y.T. Effects of ultrasonic vibration on the microstructure and tensile properties of the nano ZrB<sub>2</sub>/2024Al composites synthesized by direct melt reaction. *J. Alloys Compd.* **2016**, *668*, 121–127. [[CrossRef](#)]
11. Guo, Y.W.; Wei, W.; Shi, W.; Xue, D.; Zhou, X.R.; Wen, S.P.; Wu, X.L.; Gao, K.Y.; Huang, H.; Nie, Z.R. Selective laser melting of Er modified AlSi7Mg alloy: Effect of processing parameters on forming quality, microstructure and mechanical properties. *Mater. Sci. Eng. A* **2022**, *842*, 143085. [[CrossRef](#)]
12. Zhang, X.; Xiao, Z.; Yu, W.; Chua, C.K.; Zhu, L.; Wang, Z.; Xue, P.; Tan, S.; Wu, Y.; Zheng, H. Influence of erbium addition on the defects of selective laser-melted 7075 aluminium alloy. *Virtual Phys. Prototyp.* **2022**, *17*, 406–418. [[CrossRef](#)]
13. Geng, Y.; Jia, C.; Xu, J.; Zhang, Z.; Ju, H.; Wang, D.; Yu, L. Selective laser melting of a novel high-strength Er- and Zr-modified Al-Mn-Mg alloy. *Mater. Lett.* **2022**, *313*, 131762. [[CrossRef](#)]
14. Wang, Z.; Lin, X.; Kang, N.; Chen, J.; Tang, Y.; Tan, H.; Yu, X.; Yang, H.; Huang, W. Directed energy deposition additive manufacturing of a Sc/Zr-modified Al-Mg alloy: Effect of thermal history on microstructural evolution and mechanical properties. *Mater. Sci. Eng. A* **2021**, *802*, 140606. [[CrossRef](#)]
15. Dong, Y.; Wang, M.J.; Zhang, G.W.; Xu, H. Influence of Ti/C mass ratio on the microstructure of Al-Ti-C master alloy and refinement effect on pure aluminum. *Results Phys.* **2021**, *23*, 104000. [[CrossRef](#)]
16. Zhang, M.X.; Kelly, P.M.; Easton, M.A.; Taylor, J.A. Crystallographic study of grain refinement in aluminum alloys using the edge-to-edge matching model. *Acta Mater.* **2005**, *53*, 1427–1438. [[CrossRef](#)]
17. Kai, X.Z.; Wang, Y.H.; Chen, R.K.; Peng, Y.J.; Shi, A.J.; Tao, R.; Liang, X.F.; Li, G.R.; Chen, G.; Xu, X.J.; et al. Effects of in-situ ZrB<sub>2</sub> nanoparticles and scandium on microstructure and mechanical property of 7N01 aluminum alloy. *J. Rare Earths* **2023**. [[CrossRef](#)]
18. Liu, T.; Hu, M.L.; Li, X.J.; Piao, J.J. Synthesis of Al-5Ti-1B-1Ce alloy from remelted chips and its refinement effect. *Mater. Lett.* **2023**, *349*, 134798. [[CrossRef](#)]
19. Liao, H.B.; Mo, L.L.; Li, C.B.; Zhan, M.Y.; Du, J. Grain refinement of Mg-Al binary alloys inoculated by in-situ oxidation. *Trans. Nonferrous Met. Soc.* **2022**, *32*, 3212–3221. [[CrossRef](#)]
20. Wang, F.; Qiu, D.; Liu, Z.L.; Taylor, J.A.; Easton, M.A.; Zhang, X.M. The grain refinement mechanism of cast aluminium by zirconium. *Acta Mater.* **2013**, *61*, 5636–5645. [[CrossRef](#)]
21. Limmaneevichitr, C.; Eideh, W. Fading mechanism of grain refinement of aluminium-silicon alloy with Al-Ti-B grain refiners. *Mater. Sci. Eng. A* **2003**, *349*, 197–206. [[CrossRef](#)]
22. Qiu, D.; Taylor, J.A.; Zhang, M.X.; Kelly, P.M. A mechanism for the poisoning effect of silicon on the grain refinement of Al-Si alloys. *Acta Mater.* **2007**, *55*, 1447–1456. [[CrossRef](#)]
23. Ding, H.M.; Liu, X.F.; Yu, L.N. Influence of zirconium on grain refining efficiency of Al-Ti-C master alloys. *J. Mater. Sci.* **2007**, *42*, 9817–9821. [[CrossRef](#)]
24. Lee, Y.C.; Dahle, A.K.; StJohn, D.H.; Hutt, J.E.C. The effect of grain refinement and silicon content on grain formation in hypoeutectic Al-Si alloys. *Mater. Sci. Eng. A* **1999**, *259*, 43–52. [[CrossRef](#)]
25. Zaid, A.I.O.; Al-Qawabah, S.M.A. Effect of Zirconium Addition on the Grain Size and Mechanical Behavior of Aluminum Grain Refined by Titanium Plus Boron (Ti+B) in the as Cast and Cold Extruded Conditions. *Key Eng. Mater.* **2012**, *510–511*, 241–247. [[CrossRef](#)]
26. Johnsson, M. Influence of Zirconium on the grain refinement of Aluminum. *Z. Met.* **1994**, *85*, 786–789.
27. Hamid, A.; Ahmend, A. Effect of other element on the grain refinement of aluminum by titanium or titanium and boron. Part 2. Effect of the refractory metals vanadium, molybdenum, zirconium, tantalum. *Z. Fuer Met.* **1989**, *80*, 643–647.
28. Wang, Z.J.; Si, N.C. Synthesis and Refinement Performance of the Novel Al-Ti-B-RE Master Alloy Grain Refiner. *Rare Met. Mater. Eng.* **2015**, *44*, 2970–2975.
29. Wang, K.; Cui, C.X.; Wang, Q.; Zhao, L.C.; Hu, Y. Microstructure of Al-5Ti-1B-1RE nanoribbon and its refining efficiency on as-cast A356 alloys. *J. Rare Earths* **2013**, *31*, 313–320. [[CrossRef](#)]
30. Li, P.T.; Ma, X.G.; Li, Y.G.; Nie, J.F.; Liu, X.F. Effects of trace C addition on the microstructure and refining efficiency of Al-Ti-B master alloy. *J. Alloys Compd.* **2010**, *503*, 286–290. [[CrossRef](#)]
31. Svendsen, L.; Jarfor, A. Al-Ti-C phase diagram. *Mater. Sci. Technol.* **1993**, *9*, 948–957. [[CrossRef](#)]

32. Kearns, M.A.; Cooper, P.S. Effects of Solutes on Grain Refinement of Selected Wrought Aluminum Alloys. *Mater. Sci. Technol.* **1997**, *13*, 650–654. [[CrossRef](#)]
33. Zhao, H.L.; Song, Y.; Li, M.; Guan, S. Grain refining efficiency and microstructure of Al-Ti-C-RE master alloy. *J. Alloys Compd.* **2010**, *508*, 206–211. [[CrossRef](#)]
34. Ma, T.F.; Chen, Z.Y.; Nie, Z.R.; Huang, H. Microstructure of Al-Ti-B-Er refiner and its grain refining performance. *J. Rare Earths* **2013**, *31*, 622–627. [[CrossRef](#)]
35. Xu, C.X.; Liang, L.P.; Lu, B.F.; Zhang, J.S.; Liang, W. Effect of La on microstructure and grain-refining performance of Al-Ti-C grain refiner. *J. Rare Earths* **2006**, *24*, 596–601. [[CrossRef](#)]
36. Lai, J.; Zhang, Z.; Chen, X.G. Effect of Sc, Zr, and Ti on the interfacial reactions of the B<sub>4</sub>C/Al system. *J. Mater. Sci.* **2010**, *46*, 451–459. [[CrossRef](#)]
37. Cong, X.U.; Xiao, W.L.; Zhao, W.T.; Wang, W.; Shuji, H.; Hiroshi, Y.; Ma, C. Microstructure and formation mechanism of grain-refining particles in Al-Ti-C-RE grain refiners. *J. Rare Earths* **2015**, *33*, 553–561.
38. Corrochano, J.; Cerecedo, C.; Valcárcel, V.; Lieblich, M.; Guitián, F. Whiskers of Al<sub>2</sub>O<sub>3</sub> as reinforcement of a powder metallurgical 6061 aluminium matrix composite. *Mater. Lett.* **2008**, *62*, 103–105. [[CrossRef](#)]
39. Shen, Y.F.; Zou, Z.G.; Xiao, Z.G.; Liu, K.; Long, F.; Wu, Y. Properties and electronic structures of titanium aluminides–alumina composites from in-situ SHS process. *Mater. Sci. Eng. A* **2011**, *528*, 2100–2105. [[CrossRef](#)]
40. Ana, A.; Maria, J.A.; Rosalia, N. Alumina Whisker Selection to Design Fiber-Reinforced Polyethylene Composites. *Polym.-Plast. Technol.* **2014**, *53*, 1119–1130.
41. Sumalatha, C.; Chandra Sekhar Rao, P.V.; Subba Rao, V.V. Synthesis of nickel coated graphene and analysis of the efficacy of its reinforcement on the hyper eutectic AlSi alloys that are grain modified and refined. *Diam. Relat. Mater.* **2022**, *130*, 109519. [[CrossRef](#)]
42. Carmen, C.; Victor, V.; Monica, G.; Francisco, G. Production of Chromium-Doped  $\alpha$ -Al<sub>2</sub>O<sub>3</sub> Whiskers Via Vapor Liquid Solid Deposition. *J. Am. Ceram. Soc.* **2006**, *89*, 323–327.
43. Cui, S.; Cui, C.X.; Lv, J.; Chen, S.Y.; Xie, J.Q.; Liu, S.J. Fabrication, microstructure and mechanical properties of Al<sub>2</sub>O<sub>3</sub> whiskers reinforced Ti-46Al-4Nb alloy. *Mater. Lett.* **2020**, *259*, 126902. [[CrossRef](#)]
44. Sabuan, N.A.; Asmelash, M.; Azhari, A.; Mulubrhan, F.; Alemu, T. Investigation on the electrical conductivity of Al<sub>2</sub>O<sub>3</sub>-Ti ceramic composites using a pressureless sintering process. *Mater. Today Proc.* **2021**, *46*, 1718–1723. [[CrossRef](#)]
45. Shi, S.F.; Cho, S.H.; Goto, T.; Sekino, T. The effects of sintering temperature on mechanical and electrical properties of Al<sub>2</sub>O<sub>3</sub>/Ti composites. *Mater. Today Commun.* **2020**, *25*, 101522. [[CrossRef](#)]

**Disclaimer/Publisher’s Note:** The statements, opinions and data contained in all publications are solely those of the individual author(s) and contributor(s) and not of MDPI and/or the editor(s). MDPI and/or the editor(s) disclaim responsibility for any injury to people or property resulting from any ideas, methods, instructions or products referred to in the content.